Measurement of Myelin in the Preterm Brain: Multi-compartment Diffusion Imaging and Multi-component T_2 Relaxometry

Andrew Melbourne[1], Zach Eaton-Rosen[1], Alan Bainbridge[3], Giles S. Kendall[2], Manuel Jorge Cardoso[1], Nicola J. Robertson[2], Neil Marlow[2], and Sebastien Ourselin[1]

[1] Centre for Medical Image Computing, University College London, UK
[2] Academic Neonatology, EGA UCL Institute for Women's Health, London, UK
[3] Medical Physics, University College Hospital, London, UK

Abstract. Measurements of myelination and indicators of myelination status in the preterm brain could be predictive of later neurological outcome. Quantitative imaging of myelin could thus serve to develop predictive biomarkers; however, accurate estimation of myelin content is difficult. In this work we show that measurement of the myelin water fraction (MWF) is achievable using widely available pulse sequences and state-of-the-art algorithmic modelling of the MR imaging. We show results of myelin water fraction measurement at both 30 (4 infants) and 40 (2 infants) weeks equivalent gestational age (EGA) and show that the spatial pattern of myelin is different between these ages. Furthermore we apply a multi-component fitting routine to multi-shell diffusion weighted data to show differences in neurite density and local spatial arrangement in grey and white matter. Finally we combine these results to investigate the relationships between the diffusion and myelin measurements to show that MWF in the preterm brain may be measured alongside multi-component diffusion characteristics using clinically feasible MR sequences.

1 Introduction

Very preterm birth coincides with a period of rapid brain growth and development [1]. During the period between 30-40 weeks gestation, short range associative connections increase in number and the white matter cellular composition is altered in advance of subsequent myelination. Development of axonal myelin sheaths is fundamental to increased speed and efficiency of electrical activity in the brain and myelin related disorders are associated with a wide range of conditions. In the developing brain, processes leading to myelination progress in an established spatial pattern, ascending into the corticospinal tracts from as early as 30 weeks gestation and progressing from this region anterior and posterior over the first few months of life [2]. On magnetic resonance imaging (MRI), the absence of myelin is a major contributor to the inverted contrast, relative to the adult brain, seen on T_1 and T_2 weighted images and thus there is

K. Mori et al. (Eds.): MICCAI 2013, Part II, LNCS 8150, pp. 336–344, 2013.

interest in using MR measurement of myelin as a biomarker of later neurological outcome. Some developmental changes can be observed on diffusion weighted MRI; for instance in grey matter the increasing cortical connectivity between 30 and 40 weeks gestational age reduces the observed diffusion anisotropy in a characteristic pattern [3], but this imaging technique is mostly insensitive to myelination since the T_2 of proton spins bound into associated proteins is very short ($< 60ms$). Nonetheless, changes to the cellular content of white matter have been used to infer the presence of myelin: during the preterm period; at term equivalent age and to follow myelination through infancy [4,5].

In this work we estimate the myelin water signal from multi-echo multi-component T_2 relaxometry [6]. The multi-component T_2 sequence described in this work uses state-of-the-art MR signal modelling to iteratively estimate a B_1 inhomogeneity map and the respective T_2 component magnitudes given the applied excitation and refocusing slice profiles. In addition we constrain the component magnitudes using a preterm-specific brain segmentation routine [7] to generate a prior on the likely tissue content and search for a short T_2 component in highly anisotropic white matter regions identified by a multi-component diffusion MR sequence [8]. We show accurate component estimation in an MR gel phantom and compare results between the 30 week and 40 week equivalent gestational age (EGA) neonate brain to infer myelin content. This work, combining a practical method for myelin estimation with an existing method for fitting a multi-component diffusion model is, to the best of our knowledge, a highly novel contribution. Furthermore the application to preterm brain growth and development is of fundamental interest.

2 Methods

Single exponential fitting of multi-echo or multi echo-time (TE) data can be used to generate quantitative maps of T_2 value [4]. However, although the underlying physical T_2 relaxation processes are well described by exponential decay, complications of the image acquisition require the model-fitting be altered beyond either single or multi-exponential fitting to the data. Multi exponential decay relates the signal strength S after a number of echoes, n with multiple T_2 components of magnitudes $m(T_2)$ (1).

$$S(n) = \int m(\mathrm{T_2}) e^{-n\mathrm{TE}/\mathrm{T2}} d\mathrm{T_2} \tag{1}$$

Multi-spin echo T_2 decay generally assumes a train of perfect refocusing pulses which implies a perfectly homogenous B_1 field. In practice this condition is not met with the consequence that stimulated echoes are produced along the echo train. However, these may be modelled using the Extended Phase Graph (EPG) algorithm [9] in such a way that the local refocusing angle, α, can be estimated by simulating the history of previous imperfect refocusing pulses (2).

$$S(n) = \int \left[m(\mathrm{T_2}) \int \mathrm{EPG}(n, \mathrm{TE}, \mathrm{T_2}, \alpha(z)) dz \right] d\mathrm{T_2} \tag{2}$$

Furthermore, direct exponential fitting also implies rectangular excitation and refocusing slice profiles, a condition which is difficult to obtain. A non-rectangular slice profile introduces a non-homogenous excitation or refocusing angle across the imaging slice which results in similar effects to the stimulated echoes brought about by imperfect refocusing and thus the flip angle varies along the slice profile direction, z. If the slice pulse profile is known, this effect may also be modelled [10]. Given these considerations the multi-exponential model becomes untenable, particularly when estimating the short T_2 components that are representative of myelin content - a feature of particular interest in the developing infant brain. Thus, to obtain good estimates of local tissue T_2 composition an algorithm is required that, given the excitation and refocusing slice pulse profiles, simultaneously estimates the local field inhomogeneity and the component magnitudes. In this work we combine each of these steps to automatically estimate tissue composition from multi-echo, multi-component spin-echo T_2 relaxometry. An important addition to this procedure is the use of priors derived from an automatic adaptive tissue segmentation of the T_1-weighted data to ameliorate interaction between multi-component estimation and the slice profile correction.

To generate component magnitude priors we make use of a term equivalent age preterm-specific segmentation algorithm [7] and apply this successfully without modification to 30 week EGA infants (Figure 2). Priors are formed on the component magnitudes by propagation of the tissue class probability volumes to the T_2 space followed by Gaussian smoothing of mean, μ, and standard deviation, σ, $(N(\mu, \sigma))$ such that:

- $m_i(150ms) = P_i(\mathrm{GM}) \otimes N(0, 29ms)$,
- $m_i(225ms) = P_i(\mathrm{WM}) \otimes N(0, 29ms)$,
- $m_i(1800ms) = P_i(\mathrm{CSF}) \otimes N(0, 50ms)$,

where we initialise the white matter T_2 values from literature values [4]. In addition a prior is formed on the expected location of myelin water using additional diffusion weighted data; regions of high Fractional Anisotropy (FA) are considered likely locations for the presence of myelin. This is acceptable in the preterm brain with myelin in well defined locations, but would be inappropriate for mixed direction regions in the white matter of the myelinated adult brain.

- $m(50ms) = \mathrm{FA}_i(1 - P_i(\mathrm{GM}) \otimes N(0, 10ms))$

The prior on the low T_2 component as a function of the FA reduces the chance of generating a high myelin estimate in 30 week EGA cortical grey matter [1] (See example in Figure 1). The algorithm is illustrated in Figure 1 where after setting a predefined number of components at logarithmically spaced T_2 values between 15-2,000ms and initialising the expected refocusing angle to 180^o the algorithm iterates between estimating the component magnitudes, m_0, using (2) for a fixed refocusing angle α (maximising $p(m|\alpha)p(m|m_0)$ using the prior to form a posterior probability and using Gauss-Newton optimisation) and fixing the component magnitudes to estimate (again using (2)) the best fitting refocusing angle over

[1] FA is calculated from the extra-cellular component diffusion tensor D^* in (4).

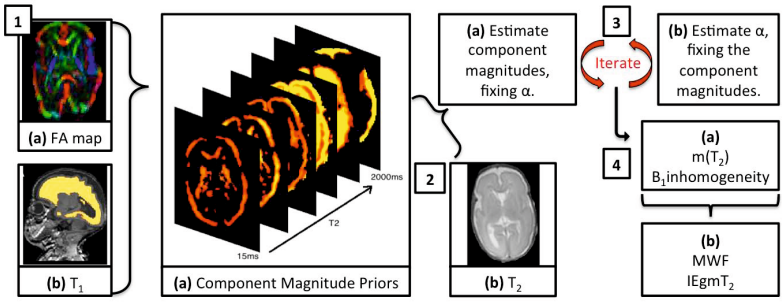

Fig. 1. Algorithm flow chart. Example using 30 week EGA infant priors. High prior component magnitude, $m(\mathrm{T}_2)$, is shown in yellow, low in red.

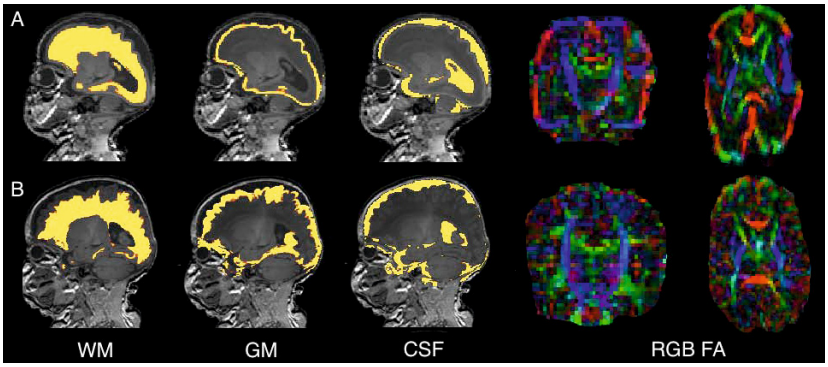

Fig. 2. Example segmentations and coronal axial colour-coded FA maps of: top row **A** 30 week (infant 2) and bottom row **B** 40 week (infant 3) EGA infants. Note the high radial cortical FA in both coronal and axial planes at 30 weeks, absent at 40 weeks [3]

a fixed range $120^o \leq \alpha \leq 180^o$ (maximising $p(\alpha|m)$). This procedure produces a component map and a B_1 inhomogeneity map. The component magnitudes are used to form a myelin water fraction (MWF) (3) [6,9].

$$\mathrm{MWF} = \frac{\int_0^{60ms} m(T_2)dT_2}{\int_0^{\infty} m(T_2)dT_2} \tag{3}$$

In addition to the multi-compartment model of myelin water described above, we also analyse data from a multi-compartment diffusion imaging model [8]. This model is fitted to two-shell diffusion weighted data to estimate neuronal cell density and likely white or grey matter dispersion by fitting of a Watson distribution to coupled intra- and extra-cellular components. This method is advantageous since it allows the local orientation and the intra and extra-cellular volume fractions to be independently correlated with the MWF.

The diffusion model combines three signal components as a function of b-value, b, and gradient direction, $\mathbf{x}$, from an isotropic space and a coupled intra

& extra cellular space (4). After constraining parallel (to the principal diffusion direction), $d_{||}$, and isotropic, d_{iso}, diffusivities, four parameters remain to be estimated: an isotropic diffusion volume fraction, v_{iso}; an intra-cellular volume fraction, v_{in} (the remaining extra-cellular volume fraction is given by $v_{ex} = 1 - v_{in} - v_{iso}$); the oblateness of the fitted Watson distribution, $0 \leq \gamma \leq 1$ (higher values tend towards a spheroid shape), used to infer white matter fibre dispersion, and the principal diffusion direction μ. Both μ and γ may be used to generate an extra-cellular component diffusion tensor D^* for which there is an analytical equivalent of the expression: $D^*(\mu, \gamma) = \int_\Omega f(\mathbf{n}|\mu, \gamma) D(\mathbf{n}) d\mathbf{n}$ when $f(\mathbf{n})$ is a Watson distribution integrated over spherical space Ω [8].

$$S(b, \mathbf{x}) = S_0 \left[v_{iso} e^{-b d_{iso}} + v_{in} \int_\Omega f(\mathbf{n}) e^{-b d_{||} (\mathbf{x} \cdot \mathbf{n})} d\mathbf{n} + v_{ex} e^{-b \mathbf{x} D^* \mathbf{x}} \right] \tag{4}$$

2.1 Data

Volumetric T_1-weighted, diffusion weighted and multi-echo T_2 data were acquired for six infants (Mean Gestational Age at Birth (GAB) of 24.9 ± 1 weeks) acquired on a Philips Achieva 3T MRI machine. Four infants were scanned at 30 weeks EGA (29+3, 30+6, 30+6, 27+5 weeks) and 2 at 40 weeks EGA (41+5, 40+5 weeks). T1 weighted data was acquired at a resolution of $0.82 \times 0.82 \times 0.5mm$ at TR/TE $=17/4.6ms$, acquisition duration $462s$. Diffusion weighted data were acquired at resolution $1.75 \times 1.75 \times 2mm$. Six volumes were acquired at b=$0s.mm^{-2}$, 16 directions at b=$750s.mm^{-2}$ and 48 directions at b=$2000s.mm^{-2}$ with TR/TE $=9s/60ms$ with total acquisition duration of $703s$. 32-echo T_2 relaxometry data were acquired at resolution $0.42 \times 0.42 \times 3mm$ with TR/TE=10s/$12ms$ and acquisition duration $700s$. Finally, we obtained data of a T_2 gel phantom using the 32-echo T_2 relaxometry sequence acquired at refocusing angle of 180^o. This phantom contains 12 gels of known T_2 ranging between $50 - 373ms$ which we additionally use to simulate multi-component gel data.

3 Results

3.1 Gel Phantom Measurements

Fitting the multi-exponential model in (1) to the gel phantom demonstrates a systematic overestimation of T_2 value[2]. Fitting the EPG algorithm (2) with known excitation and refocusing pulse profiles and variable flip-angle allows T_2 estimates with higher accuracy relative to the known gold standard, motivating the algorithm empirically in addition to theoretically. Figure 3a presents results for the first seven gels; the mean absolute difference of the exponential estimates from the gold standard over all 12 gels is $29ms$ per gel for the exponential fitting and $14ms$ per gel for the EPG fitting.

To assess the utility of the T_2 relaxometry priors, we arbitrarily mix the signal from a fixed number of gels by randomly selecting from the 12 available gels and

[2] An average T_2 value is found using $\bar{T}_2 = \int_0^\infty m(T_2) T_2 dT_2 / \int_0^\infty m(T_2) dT_2$.

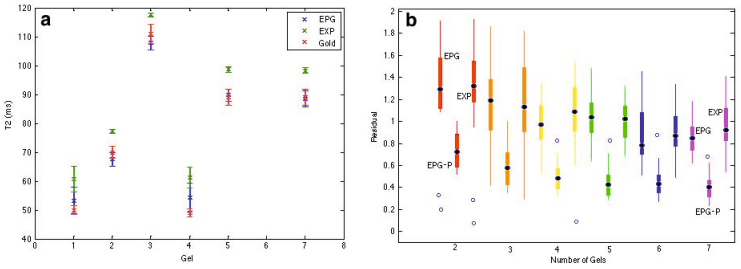

Fig. 3. Multi-component fitting to a T_2 gel phantom: **a**) Multi-exponential fitting (EXP) and multi-component EPG fitting (EPG) are shown with the known gold standard (±3%) for single gels at 296K $(GOLD)^2$; **b**) Total residual after multi-component fitting to average signal of an increasing number of randomly selected gels for EPG fitting (EPG), EPG fitting with a prior on the component magnitudes (EPG-P) and multi-exponential fitting (EXP).

fitting the multi-component model to this with and without the prior on the component magnitudes. Priors are formed by smoothing each component of the known gold standard with a Gaussian kernel of 10% of the known T_2. Figure 3b shows that the total sum of squared difference (with increasing number of gels) is lowest when using a prior on the expected T_2 component magnitudes.

3.2 Comparison of Measurements at 30 Week and 40 Week Gestational Age

Figure 4 contrasts diffusion and MWF results at 30 (top row) and 40 (bottom row) week EGA. At both ages there is the evidence of variable combinations of white matter dispersion and neurite density contributing to overlapping FA values (**a** and **e**), comparable to that found in the adult brain [8]. Furthermore, this is also true in grey matter at 30 weeks EGA (which by comparison with **e** are broadly defined as points with $v_{in} > 0.5$); high cortical FA is again a composite of high neuronal density and low dispersion - although the interpretation of dispersion is slightly different for grey as opposed to white matter. White matter dispersion values fall between 30 and 40 weeks EGA whilst FA increases. This is the first time this has been shown at these gestational ages.

Correlations between the diffusion parameters and the MWF are not obvious; voxels with high FA may have either high or low MWF. Conversely for the volume fraction, higher v_{in} implies higher FA but this can be accompanied by lower MWF. Although there is no obvious relationship between v_{in}, v_{ex} and MWF, the v_{in} distribution takes higher values at 40 weeks EGA compared to 30 weeks EGA (**b** and **f**). Again, although the number of voxels with higher values of MWF is increased at 40 weeks EGA (by 828% between 30-40wk infants, brain mask volume increase is 190%) we do not see a strong correlation with the parameters derived from the diffusion model suggesting that MWF might provide an independent measurement of white matter variability.

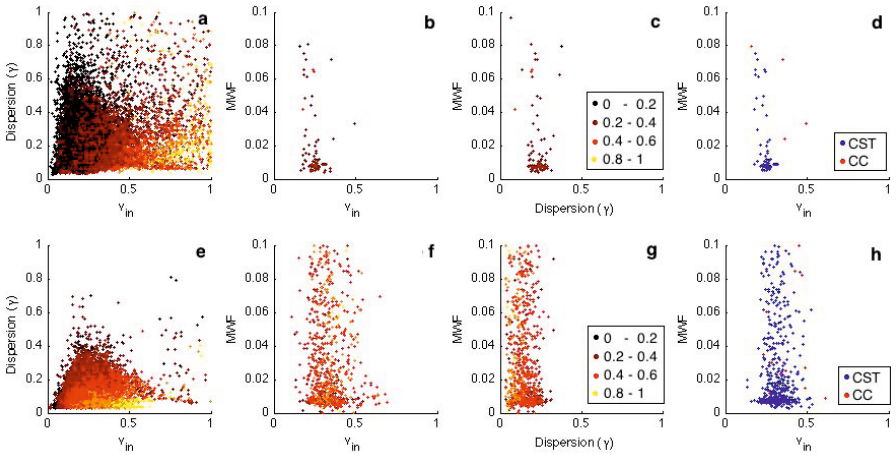

Fig. 4. a/e) diffusion dispersion vs. v_{in}, b/f) v_{in} vs. MWF, c/g) dispersion vs. MWF and d/h) v_{in} vs. MWF labelled by voxel position in the ascending CST or CC. Top row: infant at 30 week EGA; bottom row infant at 40 week EGA. Colour-coding is for FA: dark values are low FA, red/yellow values are high FA.

Figure 4 **d** and **h** label voxels by their position in either the ascending corticospinal tract (CST; blue points) or the corpus callosum (CC; red points) high MWF is strongly associated with the CST at both 30 and 40 weeks and the volume of points labelled such increases markedly (the mean MWF increases from $3.9 \pm 2\%$ to $6.8 \pm 3.5\%$ between 30 and 40 weeks EGA when fitting a Rayleigh distribution to the skewed data). Furthermore there is little evidence of any myelin presence in the CC at 30 weeks EGA and this is only lightly increased at 40 weeks EGA consistent with the known likely location of myelin at these gestational ages.

4 Discussion

This work has shown results of T_2 relaxometry that allow inference of myelin water fraction in the preterm brain [6]. Importantly the sequences used in this work are acquired in a little over 30 minutes, making this technique one that is clinically acceptable and practical. In detail, experiments of a gel phantom provided evidence that the EPG algorithm (2) can allow more accurate multi-exponential fitting (1) and that the use of priors when estimating multi-component fitting further improves accuracy. Experiments on very preterm infants at 30 and 40 weeks EGA demonstrated differences in myelin location at these ages. Furthermore the combination with a multi-component diffusion model may be used to show new relationships between white matter diffusion properties and MWF.

This work may be extended by coupling the diffusion and multi-component fitting since both sequences are based on the spin-echo describing the signal decay over time and in space. A coupled fit could even lead to combined T_2 and diffusion pulse sequences. More achievable is the modelling of myelin progression through late gestation into the preterm period. Indicators of the myelin or ongoing myelination may be correlated with functional neurodevelopment at follow up. It is interesting to note that the presence and amount of myelin can be linked via relatively simple physical models to functional measures of processing speed; quantitative estimation of myelin volume along well-defined white matter fibre pathways yields the prospect of making functional predictions. It is this potential for insight into the mechanism of neurodevelopmental deficits seen in preterm infants with abnormal MR imaging that motivates the sophisticated image analysis in this work.

In summary, widely available multi-echo image acquisitions can be used to obtain quantitative information about the preterm brain, facilitating the development of biomarkers of later functional outcome in this at risk population.

Acknowledgements. We would like to acknowledge UK registered charity SPARKS, the National Institute for Health Research (NIHR), the EPSRC (EP/H046410/1) and the UCLH/UCL Comprehensive Biomedical Research Centre Strategic Investment Award (Ref. 168).

References

1. Volpe, J.J.: Brain injury in premature infants: a complex amalgam of destructive and developmental disturbances. Lancet Neurol. 8(1), 110–124 (2009)
2. Brody, B.A., Kinney, H.C., Kloman, A.S., Gilles, F.H.: Sequence of central nervous system myelination in human infancy. i. an autopsy study of myelination. J. Neuropathol Exp. Neurol. 46(3), 283–301 (1987)
3. McKinstry, R.C., Mathur, A., Miller, J.H., Ozcan, A., Snyder, A.Z., Schefft, G.L., Almli, C.R., Shiran, S.I., Conturo, T.E., Neil, J.J.: Radial organization of developing preterm human cerebral cortex revealed by non-invasive water diffusion anisotropy MRI. Cereb. Cortex 12(12), 1237–1243 (2002)
4. Hagmann, C.F., Vita, E.D., Bainbridge, A., Gunny, R., Kapetanakis, A.B., Chong, W.K., Cady, E.B., Gadian, D.G., Robertson, N.J.: T2 at MR imaging is an objective quantitative measure of cerebral white matter signal intensity abnormality in preterm infants at term-equivalent age. Radiology 252(1), 209–217 (2009)
5. Deoni, S.C.L., Mercure, E., Blasi, A., Gasston, D., Thomson, A., Johnson, M., Williams, S.C.R., Murphy, D.G.M.: Mapping infant brain myelination with magnetic resonance imaging. J. Neurosci. 31(2), 784–791 (2011)
6. Laule, C., Leung, E., Li, D., Traboulsee, A., Patya, D., MacKay, A., Moore, G.: Myelin water imaging in multiple sclerosis: quantitative correlations with histopathology. Multiple Sclerosis 12, 747–753 (2006)
7. Cardoso, M.J., Melbourne, A., Kendall, G.S., Modat, M., Robertson, N.J., Marlow, N., Ourselin, S.: Adapt: An adaptive preterm segmentation algorithm for neonatal brain MRI. Neuroimage 65, 97–108 (2013)

8. Zhang, H., Schneider, T., Wheeler-Kingshott, C.A., Alexander, D.C.: Noddi: practical in vivo neurite orientation dispersion and density imaging of the human brain. Neuroimage 61(4), 1000–1016 (2012)
9. Prasloski, T., Maedler, B., Xiang, Q.-S., MacKay, A., Jones, C.: Applications of stimulated echo correction to multicomponent T2 analysis. Magn. Reson. Med. 67(6), 1803–1814 (2012)
10. Lebel, R.M., Wilman, A.H.: Transverse relaxometry with stimulated echo compensation. Magn. Reson. Med. 64(4), 1005–1014 (2010)